ACS APPLIED MATERIALS & INTERFACES

www.acsami.org

Research Article

Bioinspired Switchable Passive Daytime Radiative Cooling Coatings

Tiancheng Wang, Yuzhe Xiao, Jonathan L. King, Mikhail A. Kats, Kathleen J. Stebe,* and Daeyeon Lee*

Cite This: *ACS Appl. Mater. Interfaces* 2023, 15, 48716−48724

Read Online

ACCESS | Metrics & More | Article Recommendations | Supporting Information

ABSTRACT: Passive daytime radiative cooling (PDRC) relies on simultaneous reflection of sunlight and radiation toward cold outer space. Current designs of PDRC coatings have demonstrated potential as eco-friendly alternatives to traditional electrical air conditioning (AC). While many features of PDRC have been individually optimized in different studies, for practical impact, it is essential for a system to demonstrate excellence in all essential aspects, like the materials that nature has created. We propose a bioinspired PDRC structure templated by bicontinuous interfacially jammed emulsion gels (bijels) that possesses excellent cooling, thinness, tunability, scalability, and mechanical robustness. The unique bicontinuous disordered structure captures key features of Cyphochilus beetle scales, enabling a thin (130 μm) bijel PDRC coating to achieve high solar reflectance ($\gtrsim$0.97) and high longwave-infrared (LWIR) emissivity ($\gtrsim$0.93), resulting in a subambient temperature drop of ∼5.6 °C under direct sunlight. We further demonstrate switchable cooling inspired by the exoskeleton of the Hercules beetle and mechanical robustness in analogy to spongy bone structures.

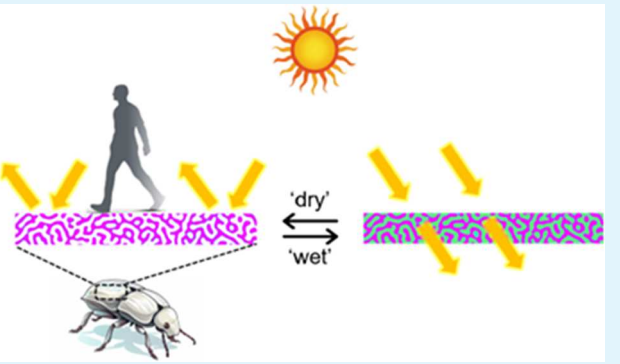

KEYWORDS: *spinodal decomposition, porous materials, disordered structure, bijels*

INTRODUCTION

Traditional electrical air conditioning (AC) systems consume significant amounts of energy and often employ coolants that pose environmental hazards.[1−3] Additionally, limited access to power infrastructure restricts AC usage in underdeveloped regions. Passive daytime radiative cooling (PDRC) coatings provide an eco-friendly and cost-effective alternative to cool surfaces and structures. PDRC coatings reduce the temperature of a surface spontaneously without energy input by reflecting solar irradiance (λ ∼0.3 to 2.5 μm) and radiating heat toward cold outer space through the long-wave infrared (LWIR) transmittance window (λ ∼8 to 13 μm).[4] The combination of high solar reflectance and LWIR emittance can yield a net temperature reduction under direct sunlight, resulting in a surface cooler than that in the ambient surroundings.

Recently, a wide range of PDRC structures have been developed, including multi-layer structures,[4−7] radiators with metallic mirrors,[9−12] particle mixtures,[8,13−15] assembled fibers,[16−22] and porous polymer films.[23−30] However, multilayer structures require time-consuming and expensive fabrication techniques; metallic mirrors are expensive and vulnerable to corrosion; particle mixtures require a polymer matrix that lowers the refractive index contrast; assembled fibers are great for self-cooling clothes, but cleaning could be an issue for long-term outdoor application. Among these, porous polymer films based on phase inversion have emerged as highly promising structures for the scalable fabrication and application of PDRC coatings. Such films of ∼300 μm thickness exhibit excellent cooling performance and offer tunable optical transmittance.[31] However, several challenges remain, including the difficulty of polymer dispersion, low mechanical strength, and a lack of structural optimization for reducing coating thickness. Ideally, a PDRC coating system would have excellent cooling performance in thin, mechanically robust layers that could switch from rejecting heat to accepting heat during periods of low sunlight and would be produced by low-cost and scalable methods.

Nature provides inspiration for addressing these challenges through the adoption of disordered, bicontinuous (disordered biphasic systems with both phases being continuous) porous structures. For instance, the bright white appearance of the Cyphochilus beetle is attributed to the unique structure of its scales. These thin scales (5−15 μm) consist of continuous, disordered, and irregular rod-shaped scattering elements that enhance light scattering efficiency by eliminating optical crowding and spatial correlations even at high volume fractions (>0.5).[32] Multiple scattering leads to high reflectance and brightness across a broad range of visible and near-infrared

Received: August 2, 2023
Accepted: September 19, 2023
Published: October 9, 2023

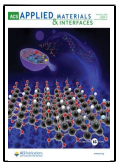

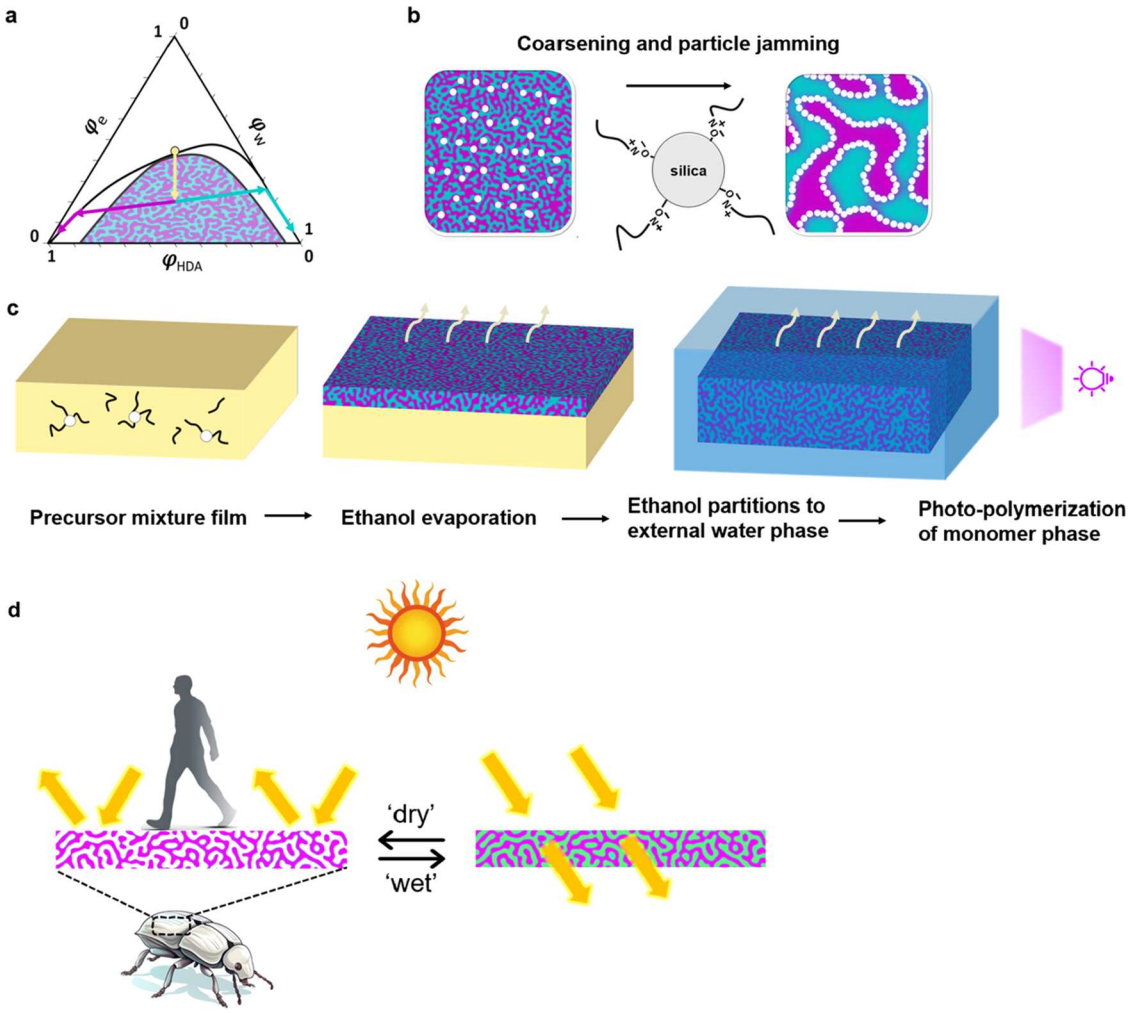

Figure 1. Bijel PDRC fabrication. (a) Representative ternary phase diagram of hexanediol diacrylate, water, and ethanol. A precursor mixture is quenched from a single-phase region into the spinodal decomposition region upon the removal of ethanol. The quenching path is indicated by a yellow arrow. (b) The interface coarsens and is stabilized by a jammed nanoparticle layer; the silica nanoparticles are modified with CTAB. (c) Two-step bijel PDRC formation via an initial VIPS step, in which a bijel outer layer is formed, followed by a STRIPS step, in which the outer layer regulates the STRIPS cosolvent removal process. (d) Schematics of the bioinspired, switchable, and mechanically robust bijel PDRC coating.

wavelengths.[33,34] In a dynamically changing environment, the Hercules beetle adapts its appearance by changing its color from green to black through the absorption of water into an open porous photonic crystal layer. This process alters the refractive index difference between the pore and solid phases, allowing the layer to reflect or transmit light.[35,36] Bicontinuous porous structures can also impart mechanical integrity. Natural bicontinuous porous structures, such as spongy bones, offer structural support and integrity under mechanical loads while maintaining low density and enabling internal mass transfer.[37−39] Importantly, the cross-linking of collagen is a key mechanism to achieving superior mechanical robustness of bones.[40]

Inspired by these examples from nature, we develop switchable, mechanically robust PDRC coatings by exploiting bicontinuous interfacially jammed emulsion gels (bijels) as templates. Bijels are particle-stabilized structures featuring two interconnected continuous liquid phases formed by arresting the spinodal decomposition of two immiscible liquid phases. The spontaneous phase separation and assembly process makes the fabrication of bijels intrinsically scalable.[41−43] Upon cross-linking of one of the two liquid phases, a porous structure with a continuous pore pervading the sample can be obtained. The continuous, disordered, and rod-like polymer domains formed through spinodal decomposition and subsequent cross-linking bear a striking resemblance to the highly reflective scales of the Cyphochilus beetle. Furthermore, the continuous pore enables the wicking of refractive index-matching fluids into the pores, thereby allowing the structure to switch its interaction with light, akin to the behavior exhibited by Hercules beetles. Because the primary application of PDRC coatings is commonly envisioned for rooftops, it is essential to consider the mechanical challenges that can arise from human and animal activities in such areas. Like bone, the bijel-templated highly cross-linked polymer and bicontinuous structure of the PDRC coating impart the necessary mechanical robustness for such applications. In addition, material selection plays a central role in PDRC coatings; optical measurement suggests that the combination of polymer and particles enhances the emissivity. Overall, bijel-templated PDRC coatings offer multiple advantages such as high solar reflectance, LWIR emissivity, switchability, scalable manufacturability, and mechanical robustness.

https://doi.org/10.1021/acsami.3c11338
ACS Appl. Mater. Interfaces 2023, 15, 48716−48724

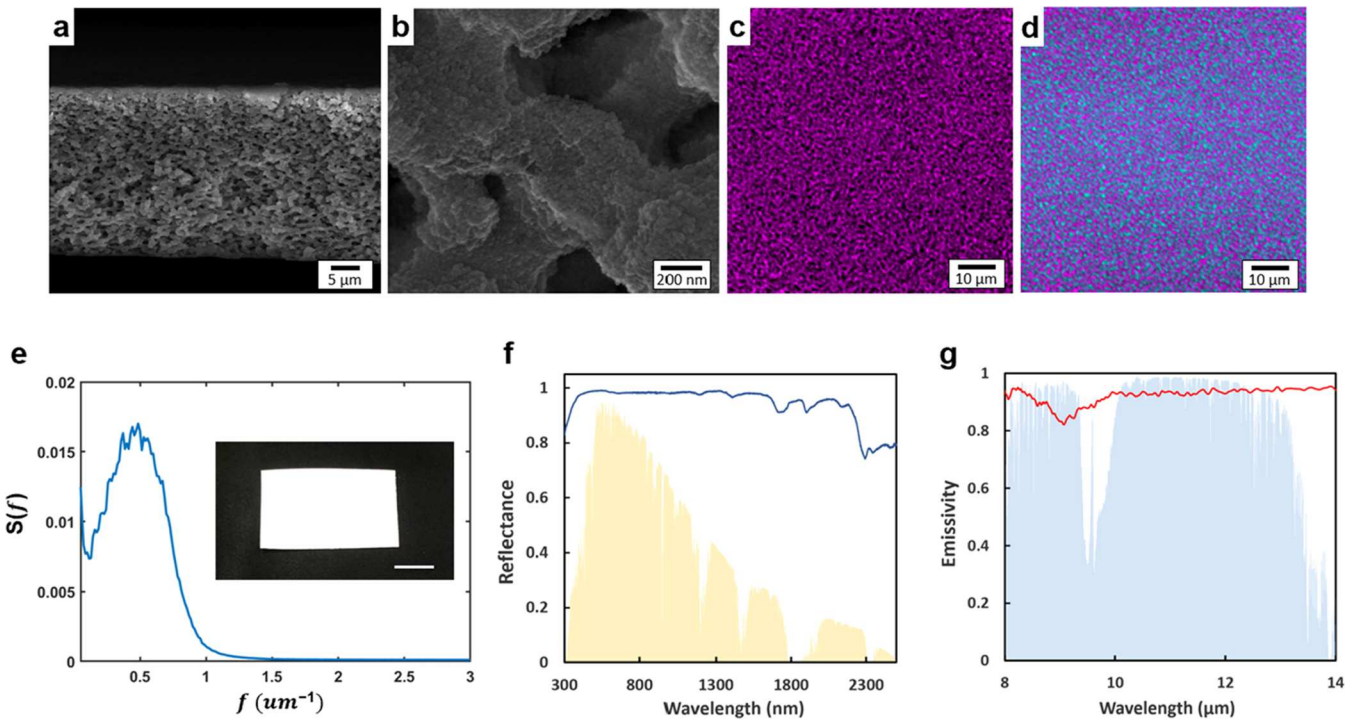

Figure 2. Structural and optical characterization of the bijel PDRC coating. (a, b) Cross-sectional scanning electron microscopy (SEM) micrographs of the polymerized bijel. (c, d) Confocal fluorescent micrographs of the bijel PDRC coating. The magenta phase is the polymer phase labeled with Nile red, and the dark/blue phase is the void phase infiltrated with dyed diethyl phthalate. (e) Radially averaged power spectra of the fluorescent micrograph of bijel structures. Inset is a macroscopic image of a 130 μm thick bijel PDRC coating, scale bar is 1 cm. (f, g) Spectral (f) reflectance and (g) emissivity of a 130 μm thick bijel PDRC coating presented against the normalized ASTM G173 Global solar spectrum and the LWIR atmospheric transparency window.

RESULTS AND DISCUSSION

Bijel PDRC coatings are fabricated with a two-step cosolvent removal process that has been introduced previously.[44] In this process, a precursor solution, consisting of a ternary mixture of two immiscible liquids, water and oil (monomer), and ethanol as a cosolvent, is used to fabricate planar bijels. In the presence of sufficient ethanol, the aqueous and oily fluids become miscible, resulting in a homogeneous single phase. The phase behavior of this mixture is illustrated in Figure 1a in a schematic ternary phase diagram. As ethanol is gradually removed, the composition of the mixture falls from the monophasic region to the spinodal region, as indicated by the yellow arrow, initiating spinodal decomposition. During phase separation, two interconnected continuous phases develop. By inducing the attachment and jamming of nanoparticles at the oil/water interface, a multiphasic composite known as a bijel can be kinetically arrested, as shown in Figure 1b. In this process, it is essential for the nanoparticles to neutrally wet both phases, allowing them to be irreversibly trapped at the interface and finally form a jammed layer as the liquid medium coarsens. In our case, we employ 22 nm silica nanoparticles combined with cetyltrimethylammonium bromide (CTAB) to adjust their wettability through electrostatic interactions. By varying the concentration of nanoparticles in the precursor mixture, the domain size can be easily controlled. Nanoparticle jamming occurs early in the phase separation process when the concentration is high, and small domains are stabilized.[45] This fine control over domain size facilitates the optimization of bijel PDRC coatings.

Figure 1c illustrates the fabrication process of a bijel PDRC coating via the vaporization-induced phase separation followed by a solvent transfer-induced phase separation (VIPS-STRIPS) process with 1,6-hexanediol diacrylate (HDA) as the oil (monomer) phase. In the VIPS step, the homogeneous precursor mixture is applied to a substrate and forms a uniform film. An air stream (5 m/s) parallel to the evaporating surface is applied to accelerate the evaporation of ethanol and a thin layer of bijel is formed via VIPS within a few seconds, while the majority of the film below the bijel layer remains homogeneous.[46] Subsequently, the entire film is immersed in water to allow further bijel formation via STRIPS as ethanol in the remaining homogeneous mixture partitions through the previously formed top bijel layer into the outer aqueous phase. As reported in our recent work, this top bijel layer regulates the ethanol flux through the tortuous channels, thereby eliminating the strong ethanol fluxes responsible for the aligned structures if only the STRIPS process is used.[47−49] After extensive, slow removal of ethanol, the bijel structure with nearly uniform domains is developed throughout the entire film. A photoinitiator present in the initial precursor mixture partitions to the HDA phase upon phase separation. With a 10 s ultraviolet (UV) irradiation, the monomer phase is polymerized to form a bicontinuous porous polymer film which spontaneously detaches from the glass substrate upon immersion in ethanol, forming a free-standing bijel PDRC film. The polymer phase is formed by cross-linking 1,6-hexanediol diacrylate. These types of acrylic polymers are widely used in industrial and consumer coatings because of their photostability and resistance to hydrolysis. As illustrated in Figure 1d, compared with current scalable porous polymer PDRC designs, bijel PDRC coatings have additional merits, including reflection-enhancing micro-

https://doi.org/10.1021/acsami.3c11338
ACS Appl. Mater. Interfaces 2023, 15, 48716−48724

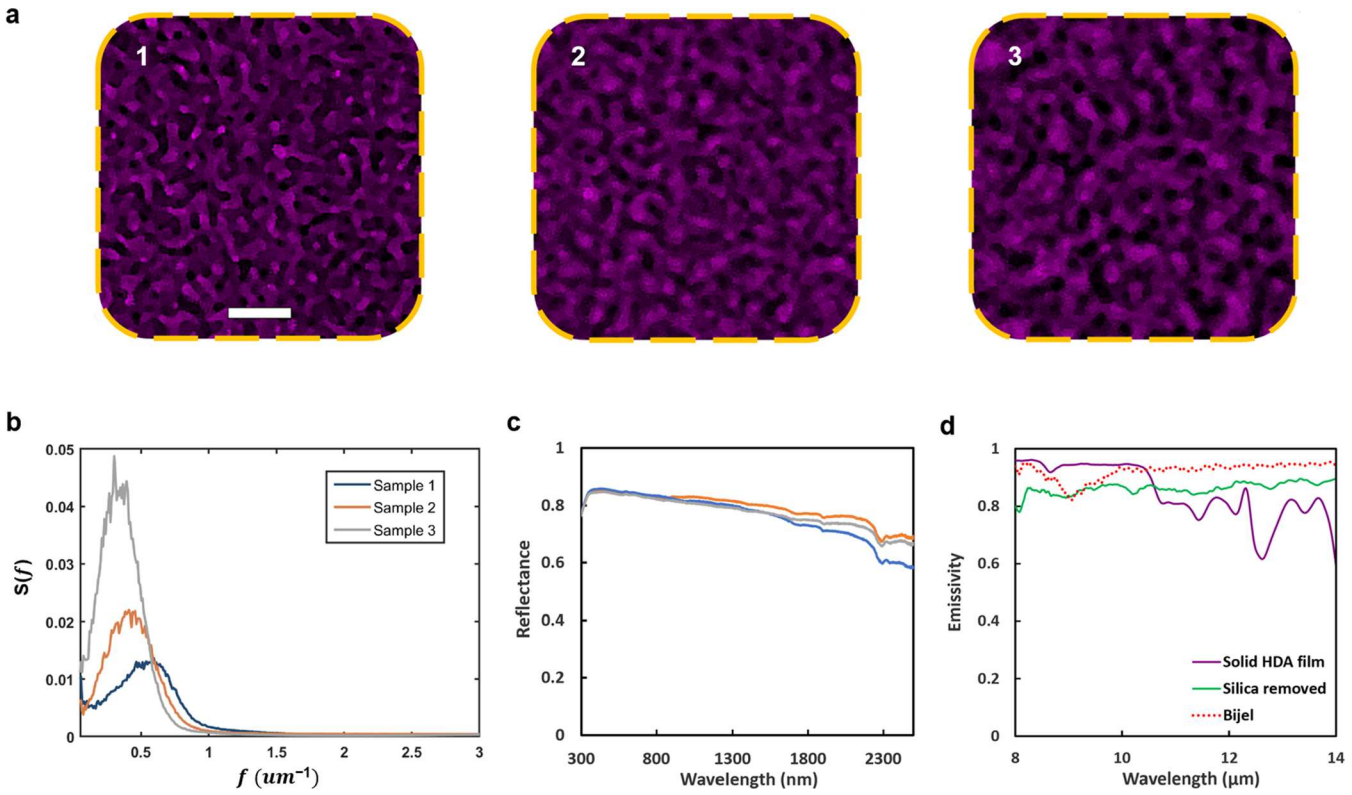

Figure 3. Structural and optical characterization of bijel PDRC coatings. (a) Confocal fluorescent micrographs of thin (30 μm) bijel PDRC coatings with increasing domain size from sample 1 to sample 3. Scale bar is 5 μm. (b) Radially averaged power spectra of samples 1, 2, and 3 in panel (a). The corresponding characteristic domain sizes are approximately 0.8, 1.2, and 1.6 μm. (c) Spectral reflectance of samples 1, 2, and 3. The corresponding measured solar reflectances are 0.831, 0.834, and 0.823, respectively. (d) Emissivity spectra of different types of samples.

structure, switchable optical responses, and mechanical robustness required in practical applications.

The structure of the resulting bijel PDRC coating is confirmed via scanning electron microscopy (SEM). The cross-sectional image in Figure 2a clearly shows the disordered and bicontinuous spinodal structures which, upon cross-linking, have formed rod-like polymer domains that resemble the microstructure of the scale of Cyphochilus beetles.[32] As the oil phase is polymerized, the jammed nanoparticle layer at the interface is locked at the polymer surface, as shown in Figure 2b. The internal structure of the bijel PDRC coating is further characterized using confocal microscopy, which allows quantitative analysis of the bijel structure. As shown in Figure 2c, the magenta phase is the polymer phase (false color) where the fluorescence comes from a hydrophobic fluorescent dye (Nile red) that was added to the precursor mixture. A dye permeation experiment is performed to examine the bicontinuity of this material. Briefly, a different fluorescent dye dissolved in diethyl phthalate permeates through the pore phase of the cross-linked bijel film. The continuity of the polymer phase (magenta) is validated by its structural integrity, whereas the permeation of the dye (blue) into all of the void space confirms the continuity of the pore phase as shown in Figure 2d. As illustrated in Figure 1d and discussed in detail below, this continuous pore phase enables switchable cooling by the introduction of index-matching fluid into the pores. Quantitative characterization of the porous structures can be conducted via either the scattering techniques[53,54] or the mathematical analysis of the imaging data. In this work, the bijel structure is characterized by performing a fast Fourier transform (FFT) analysis of confocal microscopy images. Based on the FFT analysis (see the Supporting Information for details), we estimate the characteristic feature size $\left(d = \frac{1}{2f}\right)$ to be $d \approx 1$ μm as indicated by the peak value of f around 0.5 (Figure 2e). The broad peak is a result of the disordered and irregularly shaped domains, similar to the scales of the Cyphochilus beetle.[35] The bijel PDRC coating has a bright and white appearance, as shown in the inset of Figure 2e. Unlike previously reported polymer porous film-based PDRC coatings[23−29] which typically require a thickness in the range $\gtrsim$300 μm to achieve a desired solar reflectance of $\gtrsim$0.95, bijel PDRCs of only 130 μm thickness exhibit $\gtrsim$0.97 reflectance over the solar spectrum and $\gtrsim$0.93 emissivity over the LWIR window according to the normalized ASTM G173 Global solar spectrum and the LWIR atmospheric transparency window, as shown in Figure 2f,g.

To investigate the relationship between domain size and reflectance, 30 μm thick bijel PDRC coatings with different domain sizes were prepared, as shown in Figure 3a. Based on the confocal microscopy and subsequent FFT analyses, samples 1−3 have characteristic domain sizes of around 0.8, 1.2, and 1.6 μm, respectively, as shown in Figure 3b. However, their spectral reflectances show rather minor differences (Figure 3c). Sample 2 shows the highest solar reflectance of 0.83, while sample 3 shows the lowest value of 0.82. Despite the domain size being almost doubled, the change in solar reflectance is minor. We believe that such excellent and domain-size invariant reflectance of bijel PDRC coatings within the visible/NIR range originates from their disordered bicontinuous structure, akin to the scale of the Cyphochilus beetle. More detailed studies are necessary to gain deep insight

https://doi.org/10.1021/acsami.3c11338
ACS Appl. Mater. Interfaces 2023, 15, 48716−48724

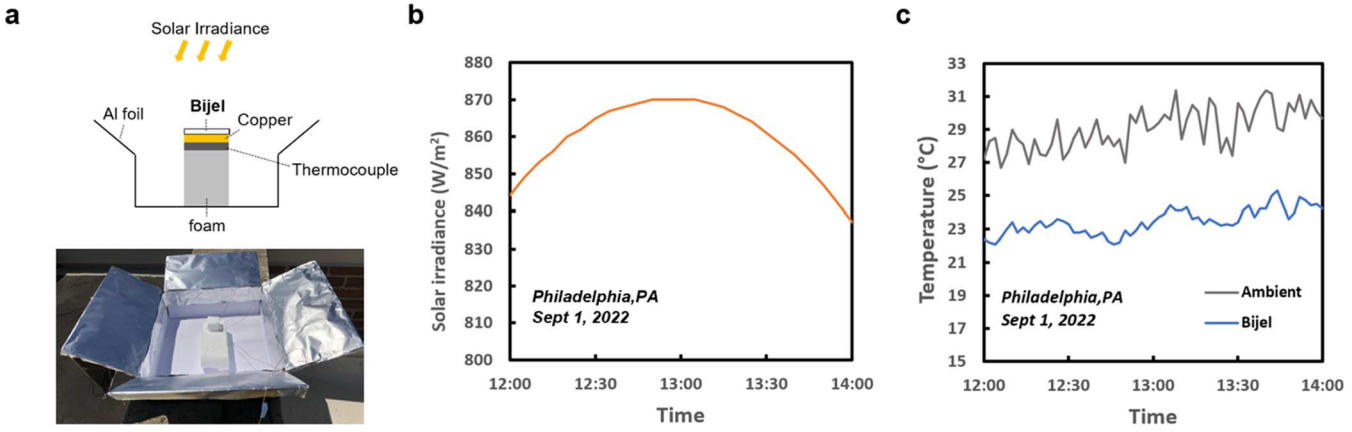

Figure 4. Passive daytime radiative cooling test. (a) Setup for a cooling test under direct sunlight. (b) Solar intensity in Philadelphia on September 1, 2022 as provided by Solcast. (c) Temperature of ambient air (gray) and bijel PDRC coating (blue) during the cooling test.

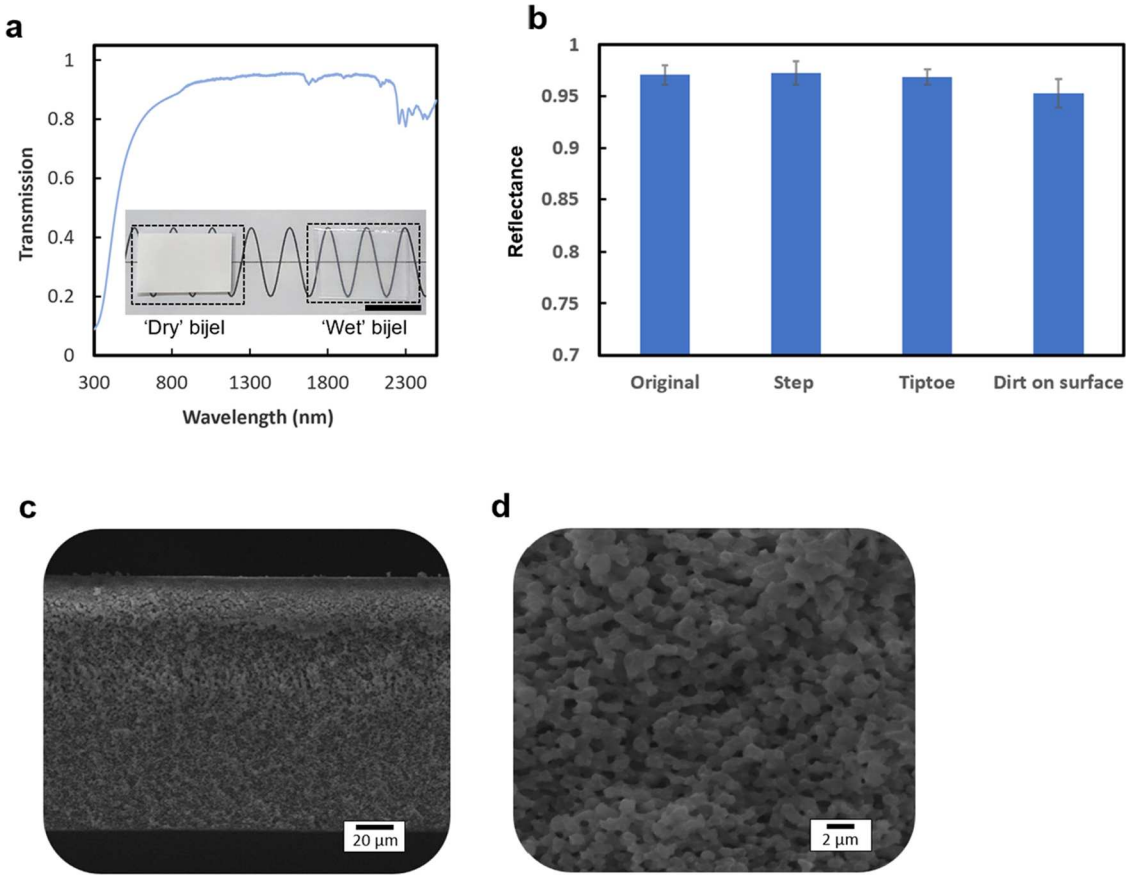

Figure 5. Tunability and mechanical robustness of bijel PDRC coatings. (a) Transmission spectrum of a bijel coating infiltrated by diethyl phthalate (DEP). The inset shows that the dry bijel coating is bright and white, while the wet bijel coating is transparent. Scale bar: 2 cm. (b) Reflectance of a bijel PDRC coating after mechanical and contamination robustness tests. (c, d) Cross-sectional SEM micrograph of a bijel PDRC coating after a "tiptoe" mechanical robustness test showing no cracks in the microstructures.

into the interactions of electromagnetic waves with such structures. One possible explanation is that the disordered and bicontinuous structure enhances the packing efficiency and, therefore, the scattering induced by individual domains.[56] Unlike most photonic structures with long-range order, insensitivity to feature sizes likely makes bijel PDRC coatings more tolerant to variations and defects that may appear during large-scale manufacturing.

While the high reflectance of the bijel PDRC coating can be attributed to the enhanced scattering originating from its structure, the high emissivity is related to its composition, including the judicious selection of polymer and nanoparticles. The C−O−C bond of the poly(HDA) phase is known to exhibit strong infrared absorption due to stretching vibrations between 770 and 1250 cm^{-1} (8−13 μm), which lies in the LWIR window. As shown in Figure 3d, a nonporous solid poly(HDA) film of 130 μm thickness exhibits high emissivity

https://doi.org/10.1021/acsami.3c11338
ACS Appl. Mater. Interfaces 2023, 15, 48716−48724

below 10 μm; however, emissivity is significantly suppressed between 10 and 13 μm, indicating that the polymer phase itself does not provide satisfactory emissivity characteristics at this thickness. By removing the silica nanoparticles from the surface of a bijel PDRC coating, we obtain a nanoparticle-free bijel film. As shown in Figure 3d, the spectral emissivity of such a sample is more uniform than that of the solid poly(HDA) film, whereas the emissivity decreased significantly compared with the original bijel PDRC coating. These observations strongly indicate that the high emissivity of the bijel PDRC coating relies on the combination of polymer, silica nanoparticle constituents, and the bijel's open porous structure. In particular, amorphous silica composed of Si−O−Si and Si−OH bonds is well-known to effectively absorb in the mid-IR (8−13 μm) region[50] while being transparent in the UV−visible range, thus avoiding undesirable heating due to absorption and enhancing the emissivity of the bijel PDRC coating.[4]

The bijel PDRC coating's performance is evaluated in a cooling test conducted under a clear sky and humidity of 38% at an ambient temperature of ∼28 °C. As shown in Figure 4a, the bijel's performance is assessed in an open system without a convection shield. The setup consists of a foam stage for insulation and a layer of Al foil as a radiation shield to block radiation from nearby buildings and other structures. During the test, under high solar intensity of ∼840−870 W/m^2, an average subambient temperature drop of ∼5.6 °C is reached below the bijel PDRC coating as shown in Figure 4b,c. While direct comparison of temperature drop of difference PDRC is not straightforward due to the differences in external variables such as humidity and air convection, it is notable that our 130 μm bijel PDRC coating's subambient cooling performance is similar to the state-of-the-art 300 μm PDRC coating based on porous poly(vinylidene fluoride-co-hexafluoropropene).[23]

Not only does the nature-inspired bijel PDRC structure provide excellent reflection and cooling performance but the bicontinuous structure also provides a continuous pore phase that can be readily filled by a liquid. When this pore phase is filled with an oil that has the same refractive index as the polymer network such as diethyl phthalate (DEP), the bijel coating switches from the bright white appearance to a nearly transparent state, as shown in Figure 5a. The transmission spectrum shows a high solar transmittance of 0.78, meaning that most of the solar irradiance penetrates through the wet bijel coating, heating both the coating and the substrate. The degree of heating will largely depend on the substrate used. As shown in the SI, once in contact with the oil, the transition from white to transparent occurs within only a few seconds as the oil permeates the bijel coating via capillarity, without the need of an external pressure. Such a fast and complete transition can be attributed to the unique continuous pore phase that acts as a smooth and uniform micrometer-size channel for capillary infiltration. The switchable bijel PDRC coating not only allows control over cooling and heating but may also be exploited in windows. To apply these bijel PDRC coatings in real applications, a strategy to encapsulate the PDRC coating in a structure with fluid reservoirs would facilitate the introduction and removal of index-matching fluid from the porous structure of the bijel.

Another important feature of bijels is their mechanical robustness. The high degree of cross-linking of the monomers in the oil phase imbues bijels with superb mechanical durability, which is essential for the application of PDRC coatings, since any deformation of the structures may greatly degrade their optical response, especially reflectance. PDRC coatings on rooftops would inevitably experience foot traffic and other mechanical loads during their lifecycle. To mimic such a situation, 135 μm thick bijel PDRC coatings with a domain size of ∼1 μm were subjected to repeated compressive loads (100 times) by a human stepping on the sample on a flat foot and on tiptoe, which translates into normal pressures of 0.15 and 1.5 MPa, respectively. Even after 100 steps, the bijel PDRC coating retains its reflectance with negligible changes, as seen in Figure 5b. Similarly, the thickness of the bijel PDRC coating remains the same (135 μm) after these tests as measured by a micrometer caliper. The cross-sectional SEM images of the bijel PDRC coating after testing show no obvious cracks as shown in Figure 5c,d. The bijel PDRC coating was also tested by subjecting it to an abrasion test by rubbing its surface against an uncleaned rooftop, which has a waterproofing polyurethane coating for a total distance of 2 m with a normal force of 1.5 N and lateral translational velocity of ∼40 cm/s. The reflectance shows a small decrease; nevertheless, the transmittance remains $\gtrsim$0.95. Considering the robustness of bijel PDRC coatings, we believe that these coatings can be applied to structures that are expected to experience repeated mechanical loads, such as rooftops and transportation vehicles. Although the sample sizes are kept small for reliable testing, bijels can be readily made in a scalable manner over a large area via roll-to-roll processing.[55]

CONCLUSIONS

Drawing inspiration from nature, we have designed and fabricated PDRC coatings with disordered and rod-like polymer domains resembling the scale of the Cyphochilus beetle, using bicontinuous interfacially jammed emulsion gels (bijels) as a template. Despite the fact that their thickness is well below those of other porous polymer PDRC coatings that have recently been developed (typically >300 μm), the disordered open porous structure of bijels leads to high reflectance; meanwhile, the high emissivity is a result of the composition of polymer and silica nanoparticles. The continuous pore phase enables the wicking of refractive index-matching fluids, allowing for switchable interactions with light. Moreover, the bicontinuous framework imparts high mechanical robustness to bijel PDRC coatings for applications in which these coatings will experience repeated mechanical loading. The ability to switch between reflecting and transmitting solar radiation, along with their scalable fabrication and excellent cooling performance, makes these bijel PDRC coatings a promising alternative to traditional air conditioning, especially in underdeveloped regions with limited access to power infrastructure. This work motivates future study on the long-term stability of bijels under prolonged solar irradiation and the impact of silica nanoparticle concentration and resultant bijel domain size on the cooling performance and mechanical durability of bijel-based PDRC coatings.

EXPERIMENTAL SECTION

Bijel PDRC Coating Fabrication. The components for precursor mixture preparation are (1) 1,6-hexanediol diacrylate (HDA), (2) concentrated Ludox TMA (50 wt % silica nanoparticle suspension in water, particles are 22 nm in diameter, pH 3), (3) pH 3 water (adjusted by 1 M HCl), (4) 200 mM cetyltrimethylammonium bromide (CTAB) solution in ethanol, (5) ethanol, and (6) 2-hydroxy-2-methylpropiophenone (HMP) as a photoinitiator. As an example,

https://doi.org/10.1021/acsami.3c11338
ACS Appl. Mater. Interfaces 2023, 15, 48716−48724

these components are mixed in the following quantities and sequence to prepare a precursor mixture: 4.6 g (1), 4.44g (4), 1.44g (5), 0.17g (3), 9.34g (2), and 0.1 g (6). The mixture is shaken and vortexed to be fully mixed. Subsequently, the sample is stored in the dark to prevent undesired photopolymerization. The resulting precursor mixture is blade-coated onto glass slides at room temperature with adjustable film thickness. To accelerate the evaporation of ethanol from the liquid precursor films, an air pipe with a control valve is used to generate airflow at velocities up to 15 m/s parallel to the evaporating surface. After 8 s of ethanol evaporation, the glass slide covered with the precursor mixture is immersed into a pH 3 water bath for 2 min. The resulting bijel film is then irradiated with ultraviolet (UV) light (25 Wm^{2-}, 340 nm) underwater for 1 min to polymerize the oil (HDA) phase. The polymerized sample on a glass slide is placed in ethanol for 10 min to make a free-standing bijel film that detaches from the glass slide. Bijel films with different feature sizes are fabricated with different CTAB concentrations in the precursor mixture. A nonporous solid poly(HDA) film is prepared by coating a HDA liquid film (contains HMP) on a glass slide, followed by 5 min of ultraviolet (UV) light irradiation. The sample of the bijel PDRC film with silica removed is prepared by immersing the bijel film in pH 13 aqueous solution of NaOH for 24 h at 60 °C. The sample is then rinsed with DI water to remove NaOH.

Fluorescence Imaging. To enable fluorescence imaging of the polymer phase, trace amounts of Nile red can be added to the precursor mixture that partitions to the oil phase upon phase separation. Further polymerization of the oil phase retains the dye inside the polymer phase. Polymerized bijel film samples are immersed in DEP for 30 min. Subsequently, a confocal microscope is used to image 2D slices of the Nile red-containing polymer film. The excitation wavelength is set to be 488 nm. For dye permeation experiments, polymerized bijel films are immersed in DEP dyed with 9,10-bis(phenylethynyl)anthracene (BPA). After 30 min, a confocal microscope is used to image the spreading of DEP in the pore phase. The excitation wavelength is set to be 488 nm. Samples are imaged with separated emission channels for the two dyes (Nile red in the polymer phase and BPA in the DEP phase): 500−530 nm for BPA and 625−725 nm for Nile red.

Optical Characterizations. The spectroscopic performance of the bijel PDRC samples was characterized separately in the UV to near-infrared (0.3−2.5 μm) and mid-infrared (8−13 μm) wavelength ranges. Spectral reflectance (0.3−2.5 μm) of bijel PDRC samples is measured using a UV−visible−near-infrared spectrophotometer (Cary 5000) equipped with a Praying mantis diffuse reflectance accessory. Optical-grade spectralon was used as the reference white material. The solar reflectance of the sample is defined by the following eq 1

$$R_{sol}(\theta) = \frac{\int_0^\infty I_{sol}(\lambda)\cdot R_{sol}(\theta, \lambda)\mathrm{d}\lambda}{\int_0^\infty I_{sol}(\lambda)\mathrm{d}\lambda} \quad (1)$$

where I_{sol} (λ) is the solar intensity spectrum (ASTM G173 Global), θ is the angle of incidence, λ is the wavelength, and R_{sol} (θ) is the angular spectral reflectance.

Direct thermal emission measurements were performed using a Bruker Vertex 70 Fourier transformed infrared (FTIR) spectrometer coupled to a Bruker Hyperion 2000 microscope with a reflective objective. A forest of vertically aligned CNTs (height ≈0.5 mm) on a silicon wafer was used as the laboratory blackbody reference. Such a blackbody reference was previously calibrated to have a roughly wavelength-independent emissivity value of about 0.97 across the mid infrared.[51] We used a Linkam THMS600 temperature-controlled stage to heat the sample and the blackbody reference to 30, 40, 50, 60, and 70 °C. Samples were placed inside the sample compartment of the FTIR with the corresponding thermal-emission signal collected by using a parabolic mirror (NA = 0.05). The emissivity of the samples measured at normal incidence are obtained from the following equation[52]

$$\varepsilon_x(\lambda) = \varepsilon_{BB}\frac{S_x(\lambda, T_1) - S_x(\lambda, T_2)}{S_{BB}(\lambda, T_1) - S_{BB}(\lambda, T_2)} \quad (2)$$

where ε_{BB} = 0.97 is the blackbody emissivity, S_x (λ, T_i) and S_{BB} (λ, T_i) are the measured thermal-emission signal from the sample (x) and blackbody reference at temperature T_i in the normal direction. Note that the final emissivity value was obtained by averaging eq 2 with different combinations of T_1 and T_2.

■ ASSOCIATED CONTENT

Supporting Information

The Supporting Information is available free of charge at https://pubs.acs.org/doi/10.1021/acsami.3c11338.

Fast Fourier transform analysis of the bijel structure; cooling performance of a DEP infiltrated bijel PDRC coating at night; angular solar reflectance of bijel PDRC coatings; binarized confocal image of bijels; rooftop conditions (PDF)

Fast infiltration of DEP into a dry bijel film (AVI)

■ AUTHOR INFORMATION

Corresponding Authors

Kathleen J. Stebe − *Department of Chemical and Biomolecular Engineering, University of Pennsylvania, Philadelphia, Pennsylvania 19104, United States;* orcid.org/0000-0003-0510-0513; Email: kstebe@seas.upenn.edu

Daeyeon Lee − *Department of Chemical and Biomolecular Engineering, University of Pennsylvania, Philadelphia, Pennsylvania 19104, United States;* orcid.org/0000-0001-6679-290X; Email: daeyeon@seas.upenn.edu

Authors

Tiancheng Wang − *Department of Chemical and Biomolecular Engineering, University of Pennsylvania, Philadelphia, Pennsylvania 19104, United States*

Yuzhe Xiao − *Department of Electrical and Computer Engineering, Department of Materials Science and Engineering, and Department of Physics, University of Wisconsin-Madison, Madison, Wisconsin 53706, United States; Department of Physics, University of North Texas, Denton, Texas 76203, United States;* orcid.org/0000-0002-0971-2480

Jonathan L. King − *Department of Electrical and Computer Engineering, Department of Materials Science and Engineering, and Department of Physics, University of Wisconsin-Madison, Madison, Wisconsin 53706, United States;* orcid.org/0000-0002-3679-5488

Mikhail A. Kats − *Department of Electrical and Computer Engineering, Department of Materials Science and Engineering, and Department of Physics, University of Wisconsin-Madison, Madison, Wisconsin 53706, United States;* orcid.org/0000-0003-4897-4720

Complete contact information is available at: https://pubs.acs.org/10.1021/acsami.3c11338

Author Contributions

T.W., D.L., and K.J.S. conceived the study. K.J.S. and D.L. supervised the experiments, while Y.X., J.K., and M.K. helped with the emissivity measurements. All authors contributed to the writing of the manuscript and participated in discussions of the research.

https://doi.org/10.1021/acsami.3c11338
ACS Appl. Mater. Interfaces 2023, 15, 48716−48724

Notes

The authors declare no competing financial interest.

■ ACKNOWLEDGMENTS

The authors acknowledge financial support from Penn MRSEC through NSF (NSF DMR 1720530 and DMR 2309043) and from NSF CBET 1945841. M.A.K. acknowledges support from the NSF (1750341). The authors thank Prof. Robert A. Riggleman for help in FFT analysis. This work was performed in part at the Singh Centerfor Nanotechnology at the University of Pennsylvania, a member of the National Nanotechnology Coordinated Infrastructure (NNCI) network, which is supported by the National Science Foundation (Grant No. NNCI-1542153). The electron microscopy facilities are supported by NSF through the University of Pennsylvania Materials Research Science and Engineering Center (MRSEC) (DMR-1720530 and DMR 2309043).

■ REFERENCES

(1) van Ruijven, B. J.; De Cian, E.; Wing, I. S. Amplification of Future Energy Demand Growth Due to Climate Change. *Nat. Commun.* **2019**, *10* (1), No. 2762, DOI: 10.1038/s41467-019-10399-3.

(2) Velders, G. J. M.; Fahey, D. W.; Daniel, J. S.; McFarland, M.; Andersen, S. O. The Large Contribution of Projected HFC Emissions to Future Climate Forcing. *Proc. Natl. Acad. Sci. U.S.A.* **2009**, *106* (27), 10949−10954.

(3) McLinden, M. O.; Brown, J. S.; Brignoli, R.; Kazakov, A. F.; Domanski, P. A. Limited Options for Low-Global-Warming-Potential Refrigerants. *Nat. Commun.* **2017**, *8* (1), No. 14476.

(4) Raman, A. P.; Anoma, M. A.; Zhu, L.; Rephaeli, E.; Fan, S. Passive Radiative Cooling below Ambient Air Temperature under Direct Sunlight. *Nature* **2014**, *515* (7528), 540−544.

(5) Rephaeli, E.; Raman, A.; Fan, S. Ultrabroadband Photonic Structures To Achieve High-Performance Daytime Radiative Cooling. *Nano Lett.* **2013**, *13* (4), 1457−1461.

(6) Chen, Z.; Zhu, L.; Raman, A.; Fan, S. Radiative Cooling to Deep Sub-Freezing Temperatures through a 24-h Day−Night Cycle. *Nat. Commun.* **2016**, *7* (1), No. 13729.

(7) Chae, D.; Kim, M.; Jung, P.-H.; Son, S.; Seo, J.; Liu, Y.; Lee, B. J.; Lee, H. Spectrally Selective Inorganic-Based Multilayer Emitter for Daytime Radiative Cooling. *ACS Appl. Mater. Interfaces* **2020**, *12* (7), 8073−8081.

(8) Zhang, H.; Ly, K. C. S.; Liu, X.; Chen, Z.; Yan, M.; Wu, Z.; Wang, X.; Zheng, Y.; Zhou, H.; Fan, T. Biologically Inspired Flexible Photonic Films for Efficient Passive Radiative Cooling. *Proc. Natl. Acad. Sci. U.S.A.* **2020**, *117* (26), 14657−14666.

(9) Zhai, Y.; Ma, Y.; David, S. N.; Zhao, D.; Lou, R.; Tan, G.; Yang, R.; Yin, X. Scalable-Manufactured Randomized Glass-Polymer Hybrid Metamaterial for Daytime Radiative Cooling. *Science* **2017**, *355* (6329), 1062−1066.

(10) Kou, J.-l.; Jurado, Z.; Chen, Z.; Fan, S.; Minnich, A. J. Daytime Radiative Cooling Using Near-Black Infrared Emitters. *ACS Photonics* **2017**, *4* (3), 626−630.

(11) Zhou, L.; Song, H.; Liang, J.; Singer, M.; Zhou, M.; Stegenburgs, E.; Zhang, N.; Xu, C.; Ng, T.; Yu, Z.; Ooi, B.; Gan, Q. A Polydimethylsiloxane-Coated Metal Structure for All-Day Radiative Cooling. *Nat. Sustainability* **2019**, *2* (8), 718−724.

(12) Yalçın, R. A.; Blandre, E.; Joulain, K.; Drévillon, J. Colored Radiative Cooling Coatings with Nanoparticles. *ACS Photonics* **2020**, *7* (5), 1312−1322.

(13) Atiganyanun, S.; Plumley, J. B.; Han, S. J.; Hsu, K.; Cytrynbaum, J.; Peng, T. L.; Han, S. M.; Han, S. E. Effective Radiative Cooling by Paint-Format Microsphere-Based Photonic Random Media. *ACS Photonics* **2018**, *5* (4), 1181−1187.

(14) Li, X.; Peoples, J.; Yao, P.; Ruan, X. Ultrawhite $BaSO_4$ Paints and Films for Remarkable Daytime Subambient Radiative Cooling. *ACS Appl. Mater. Interfaces* **2021**, *13* (18), 21733−21739.

(15) Chae, D.; Lim, H.; So, S.; Son, S.; Ju, S.; Kim, W.; Rho, J.; Lee, H. Spectrally Selective Nanoparticle Mixture Coating for Passive Daytime Radiative Cooling. *ACS Appl. Mater. Interfaces* **2021**, *13* (18), 21119−21126.

(16) Wang, X.; Liu, X.; Li, Z.; Zhang, H.; Yang, Z.; Zhou, H.; Fan, T. Scalable Flexible Hybrid Membranes with Photonic Structures for Daytime Radiative Cooling. *Adv. Funct. Mater.* **2020**, *30* (5), No. 1907562.

(17) Li, D.; Liu, X.; Li, W.; Lin, Z.; Zhu, B.; Li, Z.; Li, J.; Li, B.; Fan, S.; Xie, J.; Zhu, J. Scalable and Hierarchically Designed Polymer Film as a Selective Thermal Emitter for High-Performance All-Day Radiative Cooling. *Nat. Nanotechnol.* **2021**, *16* (2), 153−158.

(18) Zhong, H.; Li, Y.; Zhang, P.; Gao, S.; Liu, B.; Wang, Y.; Meng, T.; Zhou, Y.; Hou, H.; Xue, C.; Zhao, Y.; Wang, Z. Hierarchically Hollow Microfibers as a Scalable and Effective Thermal Insulating Cooler for Buildings. *ACS Nano* **2021**, *15* (6), 10076−10083.

(19) Zhong, S.; Yi, L.; Zhang, J.; Xu, T.; Xu, L.; Zhang, X.; Zuo, T.; Cai, Y. Self-Cleaning and Spectrally Selective Coating on Cotton Fabric for Passive Daytime Radiative Cooling. *Chem. Eng. J.* **2021**, *407*, No. 127104.

(20) Zhu, B.; Li, W.; Zhang, Q.; Li, D.; Liu, X.; Wang, Y.; Xu, N.; Wu, Z.; Li, J.; Li, X.; Catrysse, P. B.; Xu, W.; Fan, S.; Zhu, J. Subambient Daytime Radiative Cooling Textile Based on Nanoprocessed Silk. *Nat. Nanotechnol.* **2021**, *16* (12), 1342−1348.

(21) Zeng, S.; Pian, S.; Su, M.; Wang, Z.; Wu, M.; Liu, X.; Chen, M.; Xiang, Y.; Wu, J.; Zhang, M.; Cen, Q.; Tang, Y.; Zhou, X.; Huang, Z.; Wang, R.; Tunuhe, A.; Sun, X.; Xia, Z.; Tian, M.; Chen, M.; Ma, X.; Yang, L.; Zhou, J.; Zhou, H.; Yang, Q.; Li, X.; Ma, Y.; Tao, G. Hierarchical-Morphology Metafabric for Scalable Passive Daytime Radiative Cooling. *Science* **2021**, *373* (6555), 692−696.

(22) Li, J.; Liang, Y.; Li, W.; Xu, N.; Zhu, B.; Wu, Z.; Wang, X.; Fan, S.; Wang, M.; Zhu, J. Protecting Ice from Melting under Sunlight via Radiative Cooling. *Sci. Adv.* **2022**, *8* (6), No. eabj9756.

(23) Mandal, J.; Fu, Y.; Overvig, A. C.; Jia, M.; Sun, K.; Shi, N. N.; Zhou, H.; Xiao, X.; Yu, N.; Yang, Y. Hierarchically Porous Polymer Coatings for Highly Efficient Passive Daytime Radiative Cooling. *Science* **2018**, *362* (6412), 315−319.

(24) Li, T.; Zhai, Y.; He, S.; Gan, W.; Wei, Z.; Heidarinejad, M.; Dalgo, D.; Mi, R.; Zhao, X.; Song, J.; Dai, J.; Chen, C.; Aili, A.; Vellore, A.; Martini, A.; Yang, R.; Srebric, J.; Yin, X.; Hu, L. A Radiative Cooling Structural Material. *Science* **2019**, *364* (6442), 760−763.

(25) Leroy, A.; Bhatia, B.; Kelsall, C. C.; Castillejo-Cuberos, A.; Di Capua, H. M.; Zhao, L.; Zhang, L.; Guzman, A. M.; Wang, E. N. High-Performance Subambient Radiative Cooling Enabled by Optically Selective and Thermally Insulating Polyethylene Aerogel. *Sci. Adv.* **2019**, *5* (10), No. eaat9480.

(26) Zhao, H.; Sun, Q.; Zhou, J.; Deng, X.; Cui, J. Switchable Cavitation in Silicone Coatings for Energy-Saving Cooling and Heating. *Adv. Mater.* **2020**, *32* (29), No. 2000870.

(27) Gao, W.; Lei, Z.; Wu, K.; Chen, Y. Reconfigurable and Renewable Nano-Micro-Structured Plastics for Radiative Cooling. *Adv. Funct. Mater.* **2021**, *31* (21), No. 2100535.

(28) Huang, W.; Chen, Y.; Luo, Y.; Mandal, J.; Li, W.; Chen, M.; Tsai, C.; Shan, Z.; Yu, N.; Yang, Y. Scalable Aqueous Processing-Based Passive Daytime Radiative Cooling Coatings. *Adv. Funct. Mater.* **2021**, *31* (19), No. 2010334.

(29) Feng, C.; Yang, P.; Liu, H.; Mao, M.; Liu, Y.; Xue, T.; Fu, J.; Cheng, T.; Hu, X.; Fan, H. J.; Liu, K. Bilayer Porous Polymer for Efficient Passive Building Cooling. *Nano Energy* **2021**, *85*, No. 105971.

(30) Wang, T.; Wu, Y.; Shi, L.; Hu, X.; Chen, M.; Wu, L. A Structural Polymer for Highly Efficient All-Day Passive Radiative Cooling. *Nat. Commun.* **2021**, *12* (1), No. 365.

(31) Mandal, J.; Jia, M.; Overvig, A.; Fu, Y.; Che, E.; Yu, N.; Yang, Y. Porous Polymers with Switchable Optical Transmittance for Optical and Thermal Regulation. *Joule* **2019**, *3* (12), 3088−3099.
(32) Burresi, M.; Cortese, L.; Pattelli, L.; Kolle, M.; Vukusic, P.; Wiersma, D. S.; Steiner, U.; Vignolini, S. Bright-White Beetle Scales Optimise Multiple Scattering of Light. *Sci. Rep.* **2014**, *4* (1), No. 6075, DOI: 10.1038/srep06075.
(33) Zou, W.; Pattelli, L.; Guo, J.; Yang, S.; Yang, M.; Zhao, N.; Xu, J.; Wiersma, D. S. Biomimetic Polymer Film with Brilliant Brightness Using a One-Step Water Vapor−Induced Phase Separation Method. *Adv. Funct. Mater.* **2019**, *29* (23), No. 1808885.
(34) Vukusic, P.; Hallam, B.; Noyes, J. Brilliant Whiteness in Ultrathin Beetle Scales. *Science* **2007**, *315* (5810), 348.
(35) Kim, J. H.; Moon, J. H.; Lee, S.-Y.; Park, J. Biologically Inspired Humidity Sensor Based on Three-Dimensional Photonic Crystals. *Appl. Phys. Lett.* **2010**, *97* (10), No. 103701.
(36) Rassart, M.; Colomer, J.-F.; Tabarrant, T.; Vigneron, J. P. Diffractive Hygrochromic Effect in the Cuticle of the Hercules Beetle *Dynastes hercules*. *New J. Phys.* **2008**, *10* (3), No. 033014.
(37) Wang, L.; Niu, X.; Ni, Y.; Xu, P.; Liu, X.; Lu, S.; Zhang, M.; Fan, Y. Effect of Microstructure of Spongy Bone in Different Parts of Woodpecker's Skull on Resistance to Impact Injury. *J. Nanomater.* **2013**, *2013*, 1−6.
(38) Senhora, F. V.; Sanders, E. D.; Paulino, G. H. Optimally-Tailored Spinodal Architected Materials for Multiscale Design and Manufacturing. *Adv. Mater.* **2022**, *34* (26), No. 2109304.
(39) Fratzl, P.; Weinkamer, R. Nature's Hierarchical Materials. *Prog. Mater. Sci.* **2007**, *52* (8), 1263−1334.
(40) Garnero, P. The Contribution of Collagen Crosslinks to Bone Strength. *BoneKEy Rep.* **2012**, *1*, No. 182, DOI: 10.1038/bonekey.2012.182.
(41) Herzig, E. M.; White, K. A.; Schofield, A. B.; Poon, W. C. K.; Clegg, P. S. Bicontinuous Emulsions Stabilized Solely by Colloidal Particles. *Nat. Mater.* **2007**, *6* (12), 966−971.
(42) Stratford, K.; Adhikari, R.; Pagonabarraga, I.; et al. Colloidal Jamming at Interfaces: A Route to Fluid-Bicontinuous Gels. *Science* **2005**, *309* (5744), 2198−2201.
(43) Di Vitantonio, G.; Wang, T.; Stebe, K. J.; Lee, D. Fabrication and Application of Bicontinuous Interfacially Jammed Emulsions Gels. *Appl. Phys. Rev.* **2021**, *8* (2), No. 021323.
(44) Wang, T.; Riggleman, R. A.; Lee, D.; Stebe, K. J. Bicontinuous Interfacially Jammed Emulsion Gels with Nearly Uniform Sub-Micrometer Domains *via* Regulated Co-Solvent Removal. *Mater. Horiz.* **2023**, *10* (4), 1385−1391.
(45) Witt, J. A.; Mumm, D. R.; Mohraz, A. Microstructural Tunability of Co-Continuous Bijel-Derived Electrodes to Provide High Energy and Power Densities. *J. Mater. Chem. A* **2016**, *4* (3), 1000−1007.
(46) Wang, T.; Di Vitantonio, G.; Stebe, K. J.; Lee, D. Scalable Manufacturing of Hierarchical Biphasic Bicontinuous Structures via Vaporization-Induced Phase Separation (VIPS). *ACS Mater. Lett.* **2020**, *2* (5), 524−530.
(47) Haase, M. F.; Stebe, K. J.; Lee, D. Continuous Fabrication of Hierarchical and Asymmetric Bijel Microparticles, Fibers, and Membranes by Solvent Transfer-Induced Phase Separation (STRIPS). *Adv. Mater.* **2015**, *27* (44), 7065−7071.
(48) Haase, M. F.; Jeon, H.; Hough, N.; Kim, J. H.; Stebe, K. J.; Lee, D. Multifunctional Nanocomposite Hollow Fiber Membranes by Solvent Transfer Induced Phase Separation. *Nat. Commun.* **2017**, *8* (1), No. 1234.
(49) Di Vitantonio, G.; Wang, T.; Haase, M. F.; Stebe, K. J.; Lee, D. Robust Bijels for Reactive Separation *via* Silica-Reinforced Nanoparticle Layers. *ACS Nano* **2019**, *13* (1), 26−31.
(50) Jeon, S.; Son, S.; Lee, S. Y.; Chae, D.; Bae, J. H.; Lee, H.; Oh, S. J. Multifunctional Daytime Radiative Cooling Devices with Simultaneous Light-Emitting and Radiative Cooling Functional Layers. *ACS Appl. Mater. Interfaces* **2020**, *12* (49), 54763−54772.
(51) Xiao, Y.; Shahsafi, A.; Wan, C.; Roney, P. J.; Joe, G.; Yu, Z.; Salman, J.; Kats, M. A. Measuring Thermal Emission Near Room Temperature Using Fourier-Transform Infrared Spectroscopy. *Phys. Rev. Appl.* **2019**, *11* (1), No. 014026.
(52) Xiao, Y.; Wan, C.; Shahsafi, A.; Salman, J.; Yu, Z.; Wambold, R.; Mei, H.; Perez, B. E. R.; Derdeyn, W.; Yao, C.; Kats, M. A. Precision Measurements of Temperature-Dependent and Non-equilibrium Thermal Emitters. *Laser Photonics Rev.* **2020**, *14* (8), No. 1900443.
(53) Hohn, N.; Wang, X.; Giebel, M. A.; Yin, S.; Müller, D.; Hetzenecker, A. E.; Bießmann, L.; Kreuzer, L. P.; Möhl, G. E.; Yu, H.; Veinot, J. G. C.; Fässler, T. F.; Cheng, Y.-J.; Müller-Buschbaum, P. Mesoporous GeO $_x$ /Ge/C as a Highly Reversible Anode Material with High Specific Capacity for Lithium-Ion Batteries. *ACS Appl. Mater. Interfaces* **2020**, *12* (41), 47002−47009.
(54) Kreuzer, L. P.; Widmann, T.; Bießmann, L.; Hohn, N.; Pantle, J.; Märkl, R.; Moulin, J.-F.; Hildebrand, V.; Laschewsky, A.; Papadakis, C. M.; Müller-Buschbaum, P. Phase Transition Kinetics of Doubly Thermoresponsive Poly(Sulfobetaine)-Based Diblock Copolymer Thin Films. *Macromolecules* **2020**, *53* (8), 2841−2855.
(55) Siegel, H.; de Ruiter, M.; Hesseling, C. M.; Athanasiou, G.; Haase, M. F. Scalable Fabrication of Bijel Films via Continuous Flow Slit-Coating. 2023, arXiv:2301.12720. arXiv.org e-Printarchive. https://arxiv.org/abs/2301.12720.
(56) Auger, J.-C.; Martinez, V. A.; Stout, B. Theoretical Study of the Scattering Efficiency of Rutile Titanium Dioxide Pigments as a Function of Their Spatial Dispersion. *J. Coat. Technol. Res.* **2009**, *6* (1), 89−97.